

# Heat Exchanger Modelling for Solar Organic Rankine Cycle

S.M. Situmbeko\*, F.L. Inambao

*University of KwaZulu-Natal, Durban, South Africa*

---

## Abstract

The paper presents work done on the development of a heat exchanger model suitable for incorporation into a low temperature solar thermal power cycle. In particular it presents the mathematical model comprising heat transfer, mass transfer, and convective heat transfer coefficients, and velocity and pressure drop correlations for single and two phase flows. The preliminary evaporator model is based on a counter flow double pipe configuration; the flow boiling process incorporates both convective and nucleate boiling. The shell side heat transfer fluid consists of ethylene glycol at 50 % concentration; the tube side fluid flow is modelled on four candidate working fluids pre-selected from previous stages of the research study. The evaporator model is implemented on the engineering equation solver platform; following on the computer simulation results a further proposal is made for conversion of the model design into a feasible shell-and-tube heat exchanger. The outputs of the model study are in the form of the rate of heat exchange, size and type of the heat exchanger, whilst ensuring that the pressure drops and fluid velocities are within acceptable limits.

**Keywords:** *low temperature solar thermal, convective and nucleate boiling, engineering equation solver.*

---

## 1. Introduction

The paper presents research done on the design of heat exchangers for the low temperature solar thermal conversion system based on the organic Rankine cycle (ORC). Figure 1 shows the general configuration of the basic ORC cycle; the cycle constitutes three major components that involve thermal energy exchanges, being the solar collector, the evaporator and the condenser; a solar thermal conversion cycle may incorporate other types of heat exchangers such as a preheater, a superheater and a recuperator. This paper presents the development of a design model for an evaporator heat exchanger.

The evaporator heat exchanger, also known as a boiler or vapouriser, entails two types of heat exchanges, sensible and latent heat exchanges, the processes 2-3 and 3-4 respectively shown in the Temperature-entropy (T-s) diagram of figure 2. In figure 2,  $T_{H,i}$  is the temperature of the heat transfer fluid at the entrance to the heat exchanger; it can also be considered equal to the solar thermal storage temperature, assuming minimum thermal losses in the piping connecting the two

components;  $T_{H,o}$  is the return temperature of the heat transfer fluid after the heat exchange process;  $T_{H,s}$  is an arbitrary temperature along the heat transfer fluid flow stream that corresponds to the commencement of phase change along the working fluid flow stream; point 3 is otherwise also referred to as the pinch point.

## 2. Description of Model

In this part of the modelling process we develop a more detailed model of the evaporator. Specifying the heat exchanger type, materials as well as operating parameters. This information is helpful in the eventual specification of the heat exchanger to be incorporated in the solar power cycle.

The evaporator model is developed as two co-joined heat exchangers, the preheater for the sensible heating of the working fluid from the sub-cooled liquid state to the saturated liquid state and the vapouriser for the latent heating of the working liquid from the saturated liquid state to the saturated vapour state; the working fluids selected are those with near-to-isentropic turbine expansion thus not requiring superheating.

---

\* Corresponding author. Tel.: +27710570753

Fax: +27 31 260 1233; E-mail: [ssitumbeko@yahoo.com](mailto:ssitumbeko@yahoo.com)

© 2015 International Association for Sharing Knowledge and Sustainability

DOI: 10.5383/ijtee.09.01.002

The evaporator heat exchanger is initially modelled as a double pipe counter current flow heat exchanger as shown in the following figure 3; other operating parameters are also listed in table 1. In figure 3, numbers 2, 3 and 4 refer to fluid flow positions as in figures 1 and 2.

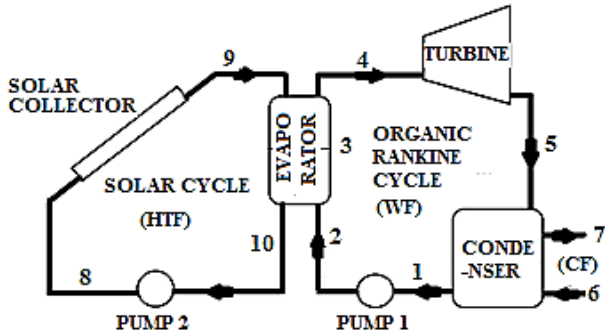


Figure 1: Heat cycle diagram [1]

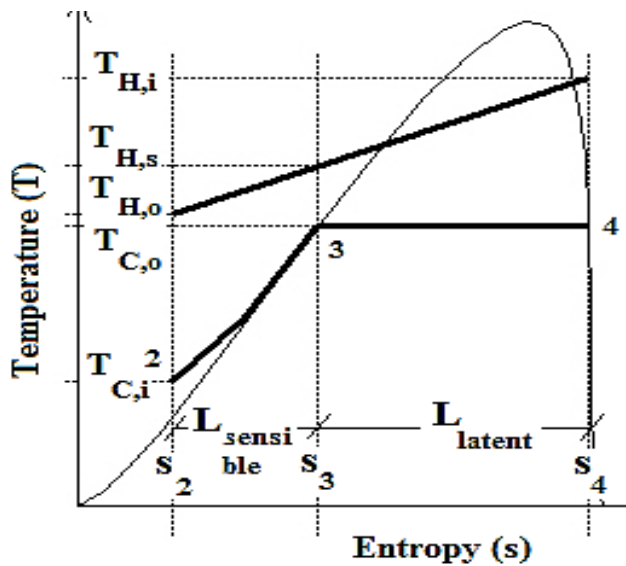


Figure 2: Temperature-Entropy diagram

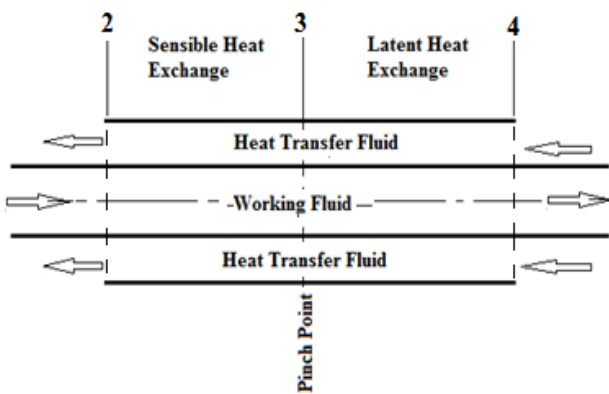


Figure 3: Evaporator heat exchanger model

The flow is assumed vertical; with the flow directions of the hot fluid (heat transfer fluid) being top-to-down in the outer pipe and that of the cold fluid (working fluid) being down-to-top in the inner pipe (refer to flow directions shown in figure 1). The complete list of model parameters is as shown in table 1 below:

Table 1: double pipe heat exchanger parameters

heat exchanger type	double pipe
flow configuration	counter flow
Thermal load required	4.2, 16.8, 84.2 kW <sub>th</sub>
Heat transfer fluid (hot stream)	ethylene glycol (50% concentration)
Working fluid (cold stream)	any of:- (i) n-butane; (ii) isobutene; (iii) R245fa; (iv) R123
tube inside diameter	20 mm (tube material: copper alloy)
tube outside diameter	23 mm (tube material: copper alloy)
shell inside diameter	34 mm (determined after parametric simulations)
heat transfer fluid mass flow rate	Varying to acceptable velocity and pressure drop
working fluid mass flow rate	varying depending on thermal load and limits for velocity and pressure drop
cooling fluid mass flow rate	varying depending on thermal load and limits for velocity and pressure drop
heat transfer fluid inlet temperature	90 °C (from solar field model)
working fluid inlet temperature	40°C
cooling fluid inlet temperature	25°C
high cycle pressure	10 atmosphere; varying to conform with heat source temperature limit
low cycle pressure	3.5 atmosphere

Heat transfer fluid used is ethylene glycol (not simply water) because the solar energy systems are located outdoors and may not be operational at night thus requiring freeze protection and/or drainage capabilities.

### 3. Mathematical Model

The evaporator was initially modelled in the first pass system model simply as a change in enthalpy as shown below: [1]

$$\frac{\dot{Q}_{\text{evap}}}{\dot{m}} = (h_{\text{out}} - h_{\text{in}}) \quad (1)$$

Where:

$\dot{Q}_{\text{evap}}$  is the rate of heat transfer from the heat transfer fluid to the working fluid in the evaporator, (W);

$\dot{m}$  is the mass flow rate of the working fluid passing through the evaporator, (kg/s);

$h_{\text{out}}$  is the enthalpy of the working fluid exiting the evaporator, (J/kg-K); and

$h_{\text{in}}$  is the enthalpy of the working fluid entering the evaporator, (J/kg-K).

In this study the mathematical model is developed as two co-joined models with common parameters at the interface, the pinch point. The model is based on the following heat exchange diagram, figure 4:

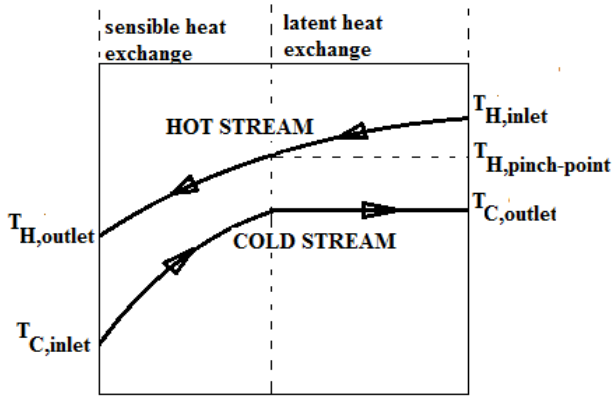


Figure 4: Heat transfer diagram

### 3.1 Sensible Heat Exchange Model

Heat transfer between the two streams can be expressed by equations 2, 3 and 4 as follows: [2]

$$Q_S = U_{S,o} A_{S,o} \Delta T_{S,LM} \quad (2)$$

where:

$Q_S$  is the heat transfer per unit time in the preheater section of the heat exchanger (W);

$A_{S,o}$  is the heat transfer area on the outer surface of the inner pipe in the preheater section of the heat exchanger ( $m^2$ );

$U_{S,o}$  is the overall heat transfer coefficient on the outer surface of the inner pipe in the preheater section of the heat exchanger ( $W/m^2$ ); and

$\Delta T_{S,LM}$  is the logarithmic mean temperature difference in the preheater section of the heat exchanger, ( $^{\circ}C$ ).

$$Q_S = \dot{m}_H C p_H (T_{H,pinch-point} - T_{H,outlet}) \quad (3)$$

$$Q_S = \dot{m}_C C p_C (T_{C,outlet} - T_{C,inlet}) \quad (4)$$

where:

$\dot{m}_H$  is the mass flow rate of the hot stream (kg/s);

$\dot{m}_C$  is the mass flow rate of the cold stream (kg/s);

$C p_H$  is the specific heat capacity of the hot stream fluid ( $J/kg-^{\circ}C$ );

$C p_C$  is the specific heat capacity of the cold stream fluid ( $J/kg-^{\circ}C$ ); and

the temperatures are as shown in figure 4.

The convective heat transfer coefficients are obtained using either the Dittus-Boelter or the Sieder and Tate correlations; the EES code checks for validity and chooses the appropriate one from the two. [3]

The Dittus-Boelter correlation is given by:

$$Nu_D = 0.023 Re_D^{0.8} Pr^n \quad (5)$$

where:

$Nu_D$  is the Nusselt number (dimensionless);

$Re_D$  is the Reynolds number (dimensionless); and

$Pr$  is the Prandtl number (dimensionless);

$n=0.4$  when fluid is being heated; and  
 $n=0.3$  when fluid is being cooled.

This correlation is valid for:

$$\left[ \begin{array}{l} 0.7 \lesssim Pr \lesssim 160 \\ Re_D \gtrsim 10000 \\ \frac{L}{D} \gtrsim 10 \end{array} \right]$$

The Sieder and Tate correlation is given by:

$$Nu_D = 0.027 Re_D^{4/5} Pr^{1/3} \left( \frac{\mu}{\mu_s} \right)^{0.14} \quad (6)$$

where:

$\mu$  is the fluid viscosity at the bulk fluid temperature ( $kg/s-m$ ); and

$\mu_s$  is the fluid viscosity at the heat-transfer boundary surface temperature ( $kg/s-m$ ).

This correlation is valid for:

$$\left[ \begin{array}{l} 0.7 \lesssim Pr \lesssim 16700 \\ Re_D \gtrsim 10000 \\ \frac{L}{D} \gtrsim 10 \end{array} \right]$$

The fouling resistances are obtained from the EES program database [4]

$R''_{fo}$ =FoulingFactor('Ethylene glycol solution')

$R''_{fi_S}$ =FoulingFactor('Refrigerant liquids')

$R''_{fi_L}$ =FoulingFactor('Refrigerant vapours')

The same fouling factors are used in the latent heat exchanger model in section 3.2.

### 3.2 Latent Heat exchange Model

In the latent section the model is segmented on account of the varying quality of the cold stream from saturated liquid to saturated vapour.

Each segment is thus modelled as:

$$Q_L[i] = U_{L,o}[i] A_{L,o}[i] \Delta T_{L,LM}[i] \quad (7)$$

$$Q_L[i] = \dot{m}_H C p_H [i] (T_{L,H}[i+1] - T_{L,H}[i]) \quad (8)$$

$$Q_L[i] = \dot{m}_C h_{fg} (x[i+1] - x[i]) \quad (9)$$

where the letters Q, U, A, ΔT, Cp, H, C and  $\dot{m}$  have the same meanings and units as in section 3.1; while L stands for latent, x for quality of the vapour (0 for saturated liquid and 1 for saturated vapour); and 'i' stands for the i-th segment.

The segmentation is made as in figure 5:

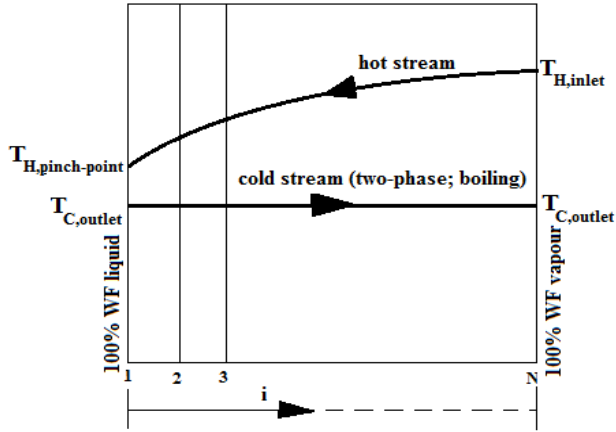


Figure 5: latent heat transfer diagram (showing segmentation direction)

The convective heat transfer coefficients for the latent heat exchange section are obtained using the Gnielinsk correlation for the hot stream and the Steiner and Taborek for the boiling stream (cold stream). Note that the Steiner and Taborek correlation also employs the Gnielinsk correlation; thus the Gnielinski correlation is given here in its general format hence the mention of liquid and vapour components.

The Gnielinsk correlation is given by:

$$\frac{h_{Lt}d_i}{k_L} = \frac{(f_L/8)(Re_{Lt}-1000)Pr_L}{1+12.7(f_L/8)^{1/2}(Pr_L^{2/3}-1)} \quad (10)$$

and the Fanning friction factor,  $f_L$ , for the liquid is:

$$f_L = [0.7904 \ln(Re_{Lt}) - 1.64]^{-2} \quad (11)$$

This expression is valid when  $4000 < Re_{Lt} < 5000000$  and  $0.5 < Pr_L < 2000$  for single-phase flows. The total mass velocity of liquid plus vapour is used for evaluating the liquid Reynolds number, so that:

$$Re_{Lt} = \frac{\dot{m}d_i}{\mu_L} \quad (12)$$

where:

- $h_{Lt}$  is the local liquid-phase forced convection coefficient based on the total flow as liquid ( $W/m^2 \cdot ^\circ C$ );
- $d_i$  is internal diameter of the pipe (m);
- $k_L$  is the local liquid-phase conductivity ( $W/m \cdot ^\circ C$ );
- $Pr_L$  is the local liquid-phase Prandtl number (-);
- $Re_{Lt}$  is the local liquid-phase Reynolds number (-);
- $\dot{m}$  is the total mass flow rate (of liquid and vapour) (kg/s); and;

$\mu_L$  is the liquid-phase viscosity at the bulk fluid temperature ( $kg/s \cdot m$ );

The Steiner and Taborek (1992) comprehensive evaporation model for flow boiling in vertical tubes based on an asymptotic approach using an exponent equal to 3 is given by: [5]

$$h_{tp} = \left[ (h_{nb,o} F_{nb})^3 + (h_{Lt} F_{tp})^3 \right]^{1/3} \quad (13)$$

where:

- $h_{tp}$  is the total boiling coefficient ( $W/m^2 \cdot ^\circ C$ );
- $h_{nb,o}$  is the local nucleate pool boiling coefficient at a reference heat flux  $q_o$  at the reduced pressure  $pr=0.1$ , ( $W/m^2 \cdot ^\circ C$ );
- $F_{nb}$  is the nucleate correction factor (but not a boiling suppression factor);
- $h_{Lt}$  is the local liquid-phase forced convection coefficient based on the total flow as liquid and is obtained with the Gnielinski (1976) correlation, ( $W/m^2 \cdot ^\circ C$ ); and
- $F_{tp}$  is the two-phase multiplier that accounts for enhancement of liquid convection by the higher velocity of a two-phase flow of a liquid in a channel.

The standard nucleate boiling coefficients for the Steiner-Taborek flow boiling correlation  $h_{nb,o}$  are provided in a table (not included in this paper) for the majority of working liquids at the following standard conditions: a reduced pressure of  $pr = 0.1$ , a mean surface roughness of  $R_{p,o} = 1 \mu m$  and the heat flux  $q_o$  equal to the value listed for each fluid. The values in this table have been calculated using the Gorenflo correlation (1993).

Some liquids are not listed in the database (table); for these, any suitable correlation may be used; in this case we used the method due to Cooper(1984), [6] to calculate the local nucleate pool boiling coefficients at reduced pressure,  $pr=0.1$ , surface roughness,  $R_p=1\mu m$ , and  $q_o$  equal  $20000 W/m^2$ , as the case is for the majority of refrigerants in the table due to Gorenflo.

The Cooper model is given by:

$$h_{nb,o} = 55 pr^{(0.12-0.4343 \ln(Rp))} (-0.4343 \ln(pr))^{-0.55} * M^{-0.5} q_o^{0.67} \quad (14)$$

where 'pr' is the reduced pressure, 'Rp' is the surface roughness and 'M' is the molar mass.

### 3.3 Pressure Drop Correlations

Pressure drop in a fluid circuit results from a number of sources such as circuit components, ducting, and accessories such as headers, manifolds and nozzles. Circuit components maybe tanks, collectors, heat exchangers etc. As the fluid has to be circulated through the circuit, it therefore means the pumping power required is associated with the pressure drop; and since pumping power has an economic factor on the circuit design, pressure drop in a heat exchanger becomes a design constraint or factor that has to be considered in heat exchanger designs.

The pressure drop in a heat exchanger is a combination of four types namely: (a) frictional losses consisting of skin friction, form drag and internal contractions and expansions; (b) momentum effects due to fluid density changes; (c) gravity effects due to changes in elevation between inlet and outlet; and (d) inlet and outlet losses due to sudden contraction and expansion at the inlet and outlet.

### 3.3.1 Single Phase Flow Pressure Drop Correlations [7]

The tube side pressure drop is given as:

$$\Delta P_t = \frac{f G_t^2 L n}{2g \rho_t d_i \Phi_t} \quad (15)$$

where:

- f is the friction factor;
- $G_t$  is the mass velocity of the fluid ( $\text{kg/s}\cdot\text{m}^2$ );
- L is the length of the tube, (m);
- g is the acceleration due to gravity, = 9.8  $\text{m/s}^2$ ;
- $\rho_t$  is the density of the fluid ( $\text{kg/m}^3$ );
- $d_i$  is the inside diameter of the tube, (m);
- n is the number of tube passes;
- $\Delta P_t$  is the pressure drop, (Pa); and

$$\Phi_t \quad \text{is the dimensionless viscosity ratio; } \Phi_t = \left(\frac{\mu_\infty}{\mu_s}\right)^{0.14};$$

where  $\mu_\infty$  the viscosity of the fluid at the bulk temperature; and  $\mu_s$  is the viscosity of the fluid at the film temperature.

In a multi-pass exchanger, in addition to frictional loss there is also a pressure drop referred to as return loss and expressed as:

$$\Delta P_r = 4n \left(\frac{V^2}{2g}\right) \rho_t \quad (16)$$

where:

- n is the number of tube passes; and
- V is the linear velocity of the tube fluid (m/s).

Thus the total tube-side pressure drop is given as:

$$\Delta P_T = \Delta P_t + \Delta P_r \quad (17)$$

For the shell side if we assume an unbaffled layout, the pressure drop is given as:

$$\Delta P_s = \frac{f_s G_s^2 L N}{2g \rho_s D_H \Phi_s} \quad (18)$$

where:

- L is the shell length, (m);
- N is the number of shell passes;
- $\rho_s$  is the shell fluid density, ( $\text{kg/m}^3$ );
- $G_s$  is the shell-side mass velocity, ( $\text{kg/m}^2\cdot\text{s}$ );
- $D_H$  is the hydraulic diameter of the shell, (m); and
- $\Phi_s$  is viscosity correction factor for shell-side fluid;

$$\Phi_s = \left(\frac{\mu_\infty}{\mu_s}\right)^{0.14} \quad (19)$$

### 3.3.2 Two Phase Flow Pressure Drop Correlations[8]

The total pressure drop in a two-phase flow can be calculated as follows:

$$\Delta p = \Delta p_s + \Delta p_f + \Delta p_m + \Delta p_g \quad (20)$$

For the tube side flow the friction pressure drop can be presented as:

$$\Delta p_f = \Delta p_{f,lo} \varphi_{lo}^2 = f_{lo} \frac{2L}{D_h} \frac{G^2}{g_c \rho_l} \varphi_{lo}^2 \quad \text{or} \quad \Delta p_f = \Delta p_{f,vo} \varphi_{vo}^2 = f_{vo} \frac{2L}{D_h} \frac{G^2}{g_c \rho_v} \varphi_{vo}^2 \quad (21)$$

where  $f_{lo}$  and  $f_{vo}$  represent the single-phase Fanning friction factor (the total mass flow rate as liquid or vapour, respectively,  $f_{lo}$  equal to  $16/\text{Re}_{lo}$  for  $\text{Re}_{lo} = GD_H/\mu_l < 2000$ , and  $f_{lo} = 0.079(\text{Re}_{lo})^{-0.25}$  for  $\text{Re}_{lo} > 2000$ ). The pressure drop two phase friction multipliers  $\varphi_{lo}^2$  and  $\varphi_{vo}^2$  are determined from some correlations such as Friedel, Chisholm, and Lockhart-Martinelli.

The momentum pressure drop can be calculated by integrating the momentum balance equation, thus obtaining:

$$\Delta p_m = \frac{G^2}{g_c} \left[ \left( \frac{x^2}{\alpha \rho_v} + \frac{(1-x)^2}{(1-\alpha)\rho_l} \right)_{z=z2} - \left( \frac{x^2}{\alpha \rho_v} + \frac{(1-x)^2}{(1-\alpha)\rho_l} \right)_{z=z1} \right] \quad (22)$$

where ‘ $\alpha$ ’ represents the void fraction of the vapour (gas) phase.

Finally, the pressure drop caused by the gravity (hydrostatic) effect is:

$$\Delta p_g = \pm \frac{g}{g_c} \sin \theta \int_o^L [\alpha \rho_v + (1-\alpha)\rho_l] dz \quad (23)$$

where the negative sign (i.e., the pressure recovery) stands for a downward flow in an inclined or vertical fluid flow.

### 3.3.3 Allowable pressure drop and velocities

Allowable pressure drop for both streams. This is a very important parameter for heat exchanger design. Generally, for liquids, a value of 0.5–0.7  $\text{kg/cm}^2$  (49.03–68.65 kPa) is permitted per shell. A higher pressure drop is usually warranted for viscous liquids, especially in the tube-side. For gases, the allowed value is generally 0.05–0.2  $\text{kg/cm}^2$  (4.903–19.61 kPa), with 0.1  $\text{kg/cm}^2$  (9.807 kPa) being typical. The velocity limits are: [9], [10]

Shell side velocity  $0.5 \leq V_s \leq 2$  (m/s)

Tube side velocity  $1 \leq V_t \leq 3$  (m/s)

## 4. Computer Simulations

Simulations are performed on the EES platform [11]; the simulation code consists of two sub-codes, one for the preheater and another for the vapouriser.

The simulations were done for each of the four candidate working fluids and for each of the three thermal loads of 4.2 kW<sub>th</sub>, 16.8 kW<sub>th</sub> and 84.2 kW<sub>th</sub> respectively representing cycles with power outputs of 0.5 kW<sub>e</sub>, 2 kW<sub>e</sub> and 10 kW<sub>e</sub>; the thermal loads were determined from cycle efficiencies in the range 10-15% obtained from the initial system model thus giving an average cycle efficiency of 12.5%. [1]

Parametric simulations were done in two runs; in the first run, the shell diameter (outer pipe was varied from an initial assumed value of 0.026m in increments of 0.002m until acceptable pressure drops and velocities were attained at 0.034m. In the second set the shell diameter was kept constant at 0.034m with tube diameters maintained at 0.020 and 0.023 m respectively for inside and outside; while the glycol mass flow rate was varied from 0.5-5 kg/s in increments of 0.5 kg/s until the code responded with a ‘non-convergence’ error message. Output parameters were mass flow rate for the working fluid, heat exchanger area and length, pressure drops and velocities, temperatures and overall heat transfer coefficients. It is also important to note that the high cycle operational pressure was constrained for each working fluid by the thermodynamic requirement that the saturation temperature must lie below the heat source temperature, 90°C; as shown in table 2; these value were determined in preliminary trial runs where the pressure was varied; the initial value of 10 atmospheres was determined from comparisons with typical operating conditions for similar cycles (10 to 30 atmospheres)[12], [13], and also with higher pressure steam cycles operating in the 100 to 300 atmospheres. [14], [15].

Table 2: high cycle pressure and saturation temperature

Working Fluid	Saturation Pressure (kPa)	Saturation Temperature (°C)
n-butane	1010	80.03
isobutane	1010	66.82
R123	506.6	81.35
R245fa	810.6	80.99

5. Results

The complete set of results is shown in the appendix. Table 3 shows the most optimal results in terms of minimum heat exchanger size that satisfies the velocity and pressure drop requirements; the results are presented for each of the three thermal loads and for each of the four working fluids. In cases where the selection requirements are not met the closest option has been selected; this is especially so with the 84.2 kW<sub>th</sub> thermal load.

Other results are shown in plots in figures 6 to 14. The plots in figures 6, 7, 8, 9, 10 and 12 show the variation of shell side pressure drop and heat exchanger length with shell side mass flow rate; figure 11 shows the variation of tube side pressure drop with shell side mass flow rate. Finally figures 13 and 14, show the variation of tube side fluid velocity and mass flow rate with thermal load.

Table 3: Summarised Heat Exchanger Design Data

Working Fluid Parameter	Thermal Load (kW <sub>th</sub> )	n-butane	isobutane	R123	R245fa
		Total Heat Exchanger Length (m)	8.758	4.114	10.901
Total Shell Side Pressure Drop (kPa)	16.8	27.398	11.423	34.02	32.020
Total Tube Side Pressure Drop (kPa)	84.2	171.41	48.790	186.02	240.57
Maximum Shell Side Velocity (m/s)	4.2	3.980	1.880	4.960	4.740
Maximum Tube Side Velocity (m/s)	16.8	12.530	5.250	15.970	14.640
	84.2	267.74	76.510	430.48	375.82
	4.2	0.002	0.001	0.004	0.003
	16.8	0.058	0.032	0.131	0.108
	84.2	6.354	2.428	12.206	14.219
	4.2	1.993	1.993	1.993	1.993
	16.8	1.993	1.993	1.993	1.993
	84.2	3.985	3.985	4.982	3.985
	4.2	0.066	0.078	0.053	0.054
	16.8	0.263	0.312	0.214	0.216
	84.2	1.317	1.566	1.070	1.080

5.1 Thermal Load: 4.2kW<sub>th</sub>

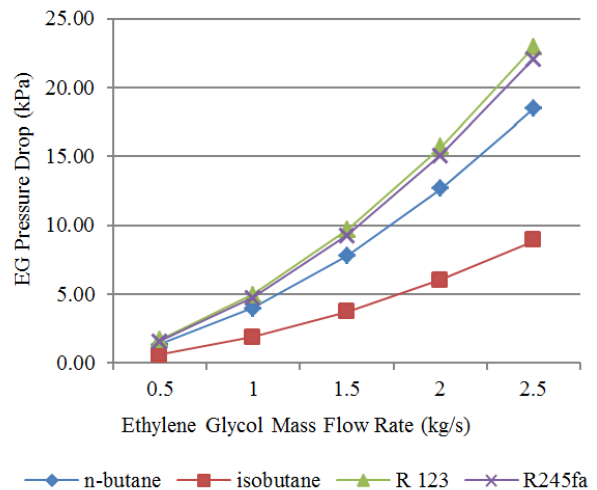


Figure 6: variation of shell side pressure drop with shell side mass flow rate for 4.2 kW<sub>th</sub> thermal load

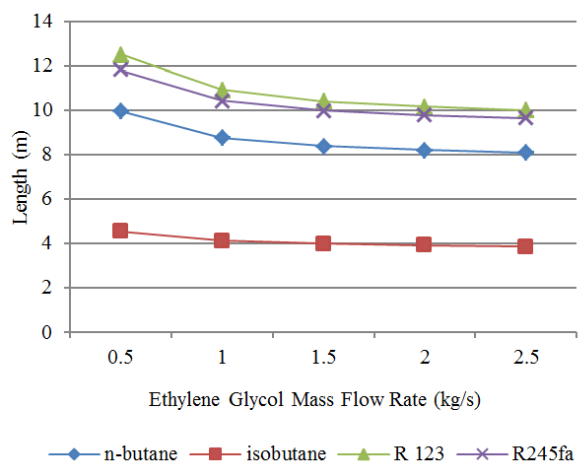


Figure 7: variation of heat exchanger length with shell side mass flow rate for 4.2 kW<sub>th</sub> thermal load

5.2 Thermal Load: 16.8kWth

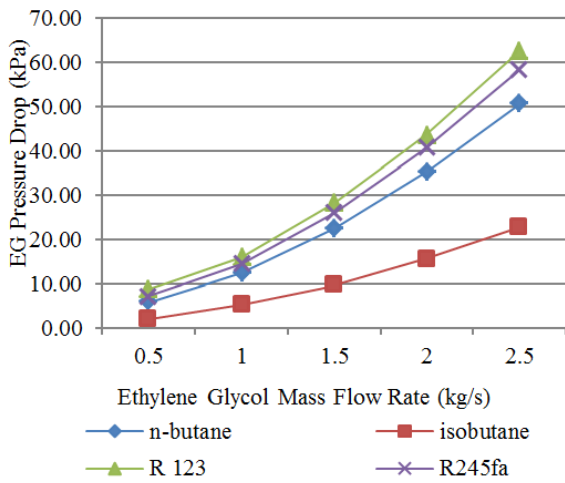


Figure 8: variation of shell side pressure drop with shell side mass flow rate for 16.8 kWth thermal load

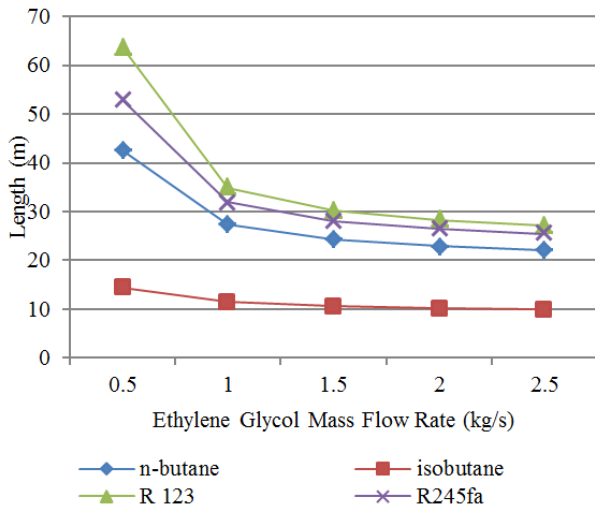


Figure 9: variation of heat exchanger length with shell side mass flow rate for 16.8 kWth thermal load

5.3 Thermal Load: 84.2kWth

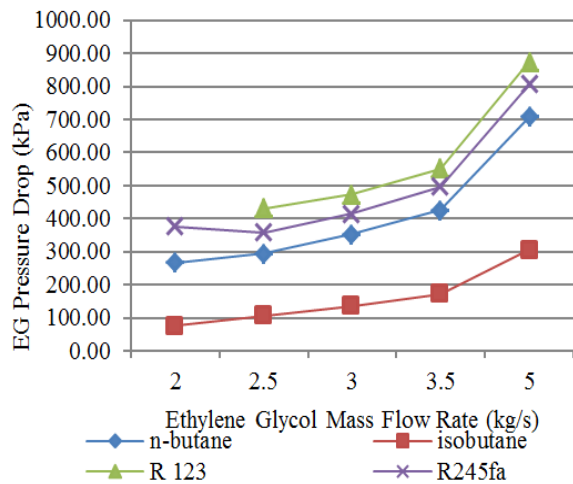


Figure 10: variation of shell side pressure drop with shell side mass flow rate for 84.2 kWth thermal load

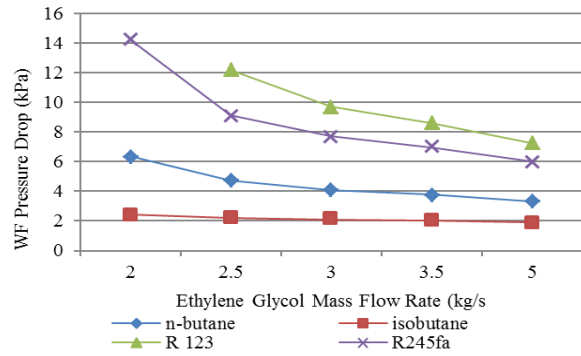


Figure 11: variation of tube side pressure drop with shell side mass flow rate for 84.2 kWth thermal load

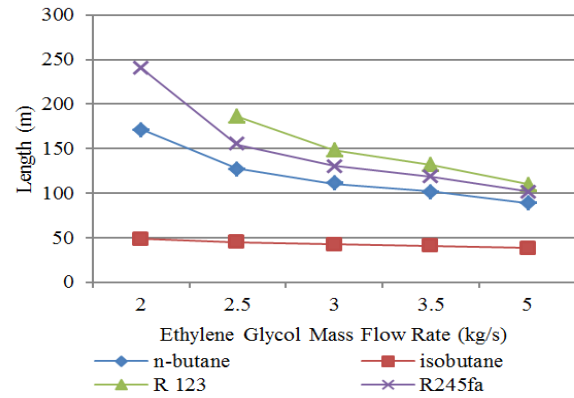


Figure 12: variation of heat exchanger length with shell side mass flow rate for 84.2 kWth thermal load

5.4 Other Results

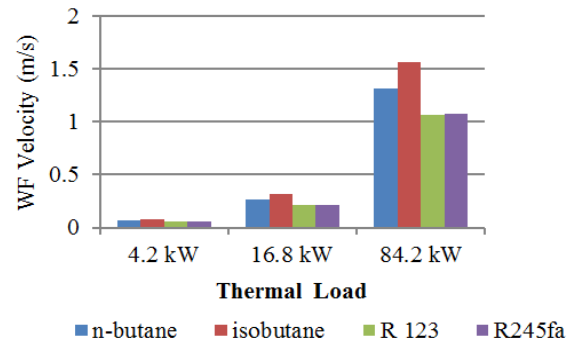


Figure 13: variation of tube side maximum velocity with working fluid type for all thermal loads

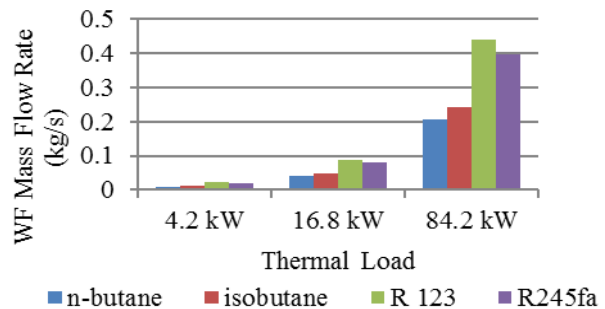


Figure 14: variation of tube mass flow rate with working fluid type for all thermal loads

## 6. Discussions

For thermal loads 4.2 and 16.8 kW<sub>th</sub> the double pipe heat exchanger is adequate in terms of both material and manufacturing costs (size) and operational costs (pressure drop and velocity limits).

For the 84.2 kW<sub>th</sub> thermal load there is need to reconfigure the heat exchanger into a shell and tube or plate heat exchanger. Assuming a tube length of 5m as acceptable a simple conversion to a single pass shell and single pass tube configuration is proposed as in table 4.

**Table 4: Preliminary heat exchanger design configurations**

Working Fluid	Preliminary Design Length (based on Double Pipe) [m]	Recommended Number of Tubes	Recommended Configuration
n-butane	171.41	35	1 shell pass & 1 tube pass; OR hairpin double pipe
Isobutane	48.79	10	1 shell pass & 1 tube pass; OR hairpin double pipe
R 123	186.02	38	1 shell pass & 1 tube pass; OR hairpin double pipe
R245fa	240.57	49	1 shell pass & 1 tube pass; OR hairpin double pipe

In terms of working fluid performance the optimal results are obtained with isobutene, followed by n-butane, and then R245fa, and finally R123. Simulations in the other cycle components such as the turbine and condenser will, however, consider all four candidate working fluids with the aim of selecting the overall optimal choice. The information obtained in this exercise will be used in evaluating performance of the heat exchanger in the Infinity IT10 mini turbine cycle validation process as well as evaluating the correlations used in the heat transfer models.

Further figures 6 to 9 show that a glycol mass flow rate of 2.5 kg/s is adequate for the two thermal loads of 4.2 and 16.8 kW<sub>th</sub> for all four working fluids both in terms of shell side pressure drops and fluid velocities; the corresponding tube side pressure drops are found to be insignificant and fluid velocities very low as can be seen from figures 11 (only showing tube side pressure drops for 84.2 kW<sub>th</sub>) and 13 respectively; the concern with extremely low tube side fluid velocities is that it may slow down or hinder optimal heat transfer. These results also show that for the two thermal loads the lowest cost of heat exchanger is that based on isobutene as the working fluid.

Figure 10 on the other hand shows that none of the models for the 84.2 kW<sub>th</sub> meets the requirements for the shell side pressure drops; it also shows that the glycol mass flow rate must range from 2 to 5 kg/s in order to satisfy the thermal load. The models produced prohibitive pressure drops ranging from 250 to 900 kPa for the other three working fluids, other than isobutene and it was on the account of such excessive pumping requirements that table 4 was generated proposing a rethink of the heat exchanger models for this thermal load.

The mass flow rates for the working fluids determined by the parametric analyses for the three thermal loads are shown in figure 14; the actual figures are 0.010 kg/s, 0.041 kg/s and 0.207 kg/s respectively for 4.2, 16.8 and 84.2 kW<sub>th</sub> for n-butane; the corresponding values for isobutene are 0.012, 0.048 and 0.241 kg/s; for R123 they are 0.022, 0.088 and 0.440 kg/s; and finally for R245fa they are 0.020, 0.079 and 0.396 kg/s. The lowest working fluid mass flow rates are attained with n-butane, followed by isobutene whilst R123 requires the highest mass flow rates followed by R245fa.

## 7. Conclusions and Recommendations

A heat exchanger model for the low temperature solar thermal organic Rankine cycle has been developed and evaluated on the EES platform. Parameters considered included heat exchanger size, pressure drop and fluid velocity on both the tube and shell sides. Reference values have been based on the tubular exchanger manufacturers association (TEMA) standards. Results have been analysed and discussed. The results have shown that models developed with isobutene as the working fluid are the most optimal from the four candidate working fluids tested. Further evaluations of the models and the correlations will be performed with the validation of the Infinity IT10 mini turbine ORC cycle.

Further the models developed satisfy the thermal loads, pressure drops and fluid velocities for the 4.2 and 16.8 kW<sub>th</sub> loads. On account of very high pressure drops and therefore costly pumping requirements it has been proposed to redesign the heat exchanger model for the 84.2 kW<sub>th</sub> to a multi-tube shell and tube heat exchanger.

It has also been established that a further conceptual investigation of two phase flow pressure drop be undertaken to fully appreciate its effect on the development of the heat exchanger models.

## Acknowledgments

The authors would like to thank the Centre for Engineering Postgraduate Studies (CEPS) at University of KwaZulu-Natal for providing funds for certain aspects of the research as well as all colleagues, postgraduate students and staff of the section

## References

- [1] Situmbeko S. M., Inambao F. L. Mathematical Modelling and Simulation of Low Temperature Solar Thermal Energy Conversion Systems. Proceedings of Solar World Congress. Kassel, Germany, 2011.
- [2] Thirumaleshwars M. Software Solutions to Problems of Heat Transfer, Heat Exchangers. ISBN 978-87-403-0578-4, Bookboon.com, 2013.
- [3] Incropera F.P. et al. Fundamentals of Heat and Mass Transfer. John Wiley & Sons. USA, 2007.
- [4] EES32\Userlib\HeatTransfer\FoulingFactors\FoulingFactor.lkt. 2013.
- [5] Thome J.R. Engineering Data Book III; chapter 10: Fundamentals of Evaporation in Plain Tubes, Laboratory of Heat and Mass Transfer. Swiss Federal Institute of Technology. Lausanne, Switzerland.
- [6] Thome J.R. Engineering Data Book III; chapter 9: Fundamentals of Boiling on Tubes and Tube Bundles, Laboratory of Heat and Mass Transfer, Swiss Federal Institute of Technology. Lausanne, Switzerland.

- [7] Website: [slideshare.net/rijumoniboro/heat-exchangers-12606868](http://slideshare.net/rijumoniboro/heat-exchangers-12606868)
- [8] Website: [razifar.com/cariboost\\_files/Heat\\_20 Exchangers.pdf](http://razifar.com/cariboost_files/Heat_20_Exchangers.pdf)
- [9] Website: [unix.ecs.umass.edu/~rlaurenc/Courses/che333/Reference/exchanger.pdf](http://unix.ecs.umass.edu/~rlaurenc/Courses/che333/Reference/exchanger.pdf)
- [10] Perry R.H. et al. Perry's Chemical Engineers' Handbook. 7th Edition, McGraw-Hill, 1999
- [11] Klein S.A., and Alvarado F.L. Engineering Equation Solver for Microsoft Windows Operating Systems. F-Chart Software, Middleton, USA. 2013
- [12] Website: [honeywell-refrigerants.com/Europe; honeywell-genetron-245a-orc-systems-brochure](http://honeywell-refrigerants.com/Europe;honeywell-genetron-245a-orc-systems-brochure)
- [13] Website: [infinityturbine.com](http://infinityturbine.com) – ORC Waste Heat Turbine
- [14] Website: [energy.siemens.com](http://energy.siemens.com) - power-generation steam turbines, SST-6000 Brochure, T\_6000\_Series\_Datasheet.pdf
- [15] Website: [energy.siemens.com](http://energy.siemens.com), power-generation steam turbines, SST-300.pdf

Appendix: Simulation Results

Latent IIX Section 2 Overall Heat Transfer Coefficient	Latent IIX Section 1 Overall Heat Transfer Coefficient	Sensible IIX Overall Heat Transfer Coefficient	Working Fluid Boiling Temperature	Heat Transfer Fluid Pinch Point Temperature	Heat Transfer Fluid outlet Temperature	Working Fluid Velocity	Heat Transfer Fluid Maximum Velocity	Total IIX Tube Pressure Drop	Total IIX Shell Pressure Drop	Total IIX Length	Latent IIX Length	Sensible IIX Length	Latent Thermal Load	Sensible Thermal Load	Total Thermal Load	High Pressure	Heat Transfer Fluid Mass Flow Rate	Working Fluid Mass Flow Rate	Working Fluid
[Wm <sup>2</sup> -C]	[Wm <sup>2</sup> -C]	[Wm <sup>2</sup> -C]	[C]	[C]	[C]	[m/s]	[m/s]	[kPa]	[kPa]	[m]	[m]	[m]	[W]	[W]	[W]	[kPa]	[kg/s]	[kg/s]	
1207	824.1	139.2	80.03	88.33	87.68	0.06569	0.9964	0.0019	1.35	9.927	4.729	5.198	3023	1177	4200	1.01E+06	0.5	0.01032	n-butano
1395	944.2	141.8	80.03	89.16	88.84	0.06569	1.993	0.0017	3.98	8.758	3.907	4.851	3023	1177	4200	1.01E+06	1	0.01032	n-butano
1475	994.5	142.8	80.03	89.44	89.23	0.06569	2.989	0.0016	7.78	8.383	3.643	4.74	3023	1177	4200	1.01E+06	1.5	0.01032	n-butano
1521	1023	143.3	80.03	89.58	89.42	0.06569	3.985	0.0016	12.65	8.196	3.511	4.685	3023	1177	4200	1.01E+06	2	0.01032	n-butano
1551	1041	143.7	80.03	89.67	89.54	0.06569	4.982	0.0015	18.53	8.082	3.43	4.652	3023	1177	4200	1.01E+06	2.5	0.01032	n-butano
1207	839.9	334.9	80.03	83.3	80.68	0.2628	0.9964	0.0899	5.86	42.52	29.41	13.11	12091	4709	16800	1.01E+06	0.5	0.04129	n-butano
1395	969.1	351.9	80.03	86.65	85.35	0.2628	1.993	0.0578	12.53	27.398	18.2	9.198	12091	4709	16800	1.01E+06	1	0.04129	n-butano
1475	1024	358.5	80.03	87.77	86.9	0.2628	2.989	0.0512	22.58	24.254	15.89	8.364	12091	4709	16800	1.01E+06	1.5	0.04129	n-butano
1521	1055	362	80.03	88.33	87.68	0.2628	3.985	0.0482	35.35	22.863	14.87	7.993	12091	4709	16800	1.01E+06	2	0.04129	n-butano
1551	1075	364.2	80.03	88.66	88.14	0.2628	4.982	0.0465	50.68	22.062	14.28	7.782	12091	4709	16800	1.01E+06	2.5	0.04129	n-butano
1521	1300	790	80.03	81.6	78.31	1.317	3.985	6.354	267.74	171.41	135.5	35.91	60599	23601	84200	1.01E+06	2	0.207	n-butano
1551	1324	802.2	80.03	83.29	80.66	1.317	4.982	4.717	294.54	127.29	99.81	27.48	60599	23601	84200	1.01E+06	2.5	0.207	n-butano
1572	1341	810.7	80.03	84.41	82.22	1.317	5.978	4.1027	353.76	110.72	86.59	24.13	60599	23601	84200	1.01E+06	3	0.207	n-butano
1588	1353	817	80.03	85.21	83.33	1.317	6.975	3.7671	427.29	101.7	79.44	22.26	60599	23601	84200	1.01E+06	3.5	0.207	n-butano
1619	1377	828.8	80.03	86.65	85.34	1.317	9.964	3.2975	706.91	89.04	69.45	19.59	60599	23601	84200	1.01E+06	5	0.207	n-butano
1207	746.2	107.4	81.35	88.24	87.68	0.05339	0.9964	0.0043	1.70	12.499	6.237	6.262	3175	1025	4200	506625	0.5	0.02192	R 123
1395	857.3	109	81.35	89.12	88.84	0.05339	1.993	0.0037	4.96	10.901	5.075	5.826	3175	1025	4200	506625	1	0.02192	R 123
1475	903.5	109.6	81.35	89.41	89.23	0.05339	2.989	0.0036	9.65	10.402	4.712	5.69	3175	1025	4200	506625	1.5	0.02192	R 123
1521	929.4	109.9	81.35	89.56	89.42	0.05339	3.985	0.0035	15.66	10.154	4.531	5.623	3175	1025	4200	506625	2	0.02192	R 123
1551	946.2	110.1	81.35	89.65	89.54	0.05339	4.982	0.0034	22.93	10.004	4.422	5.582	3175	1025	4200	506625	2.5	0.02192	R 123
1207	810.4	271.2	81.35	82.96	80.68	0.2136	0.9964	0.2396	8.77	63.68	46.4	17.28	12699	4101	16800	506625	0.5	0.0877	R 123
1395	925.1	282.3	81.35	86.49	85.35	0.2136	1.993	0.1312	15.97	34.93	24.04	10.89	12699	4101	16800	506625	1	0.0877	R 123
1475	974.4	286.5	81.35	87.66	86.9	0.2136	2.989	0.1138	28.19	30.299	20.51	9.789	12699	4101	16800	506625	1.5	0.0877	R 123
1521	1002	288.8	81.35	88.24	87.68	0.2136	3.985	0.1063	43.80	28.328	19.01	9.318	12699	4101	16800	506625	2	0.0877	R 123
1551	1020	290.2	81.35	88.59	88.14	0.2136	4.982	0.1022	62.52	27.225	18.17	9.055	12699	4101	16800	506625	2.5	0.0877	R 123
1551	1322	694.6	81.35	82.95	80.66	1.07	4.982	12.206	430.48	186.02	152.1	33.92	63647	20553	84200	506625	2.5	0.4395	R 123
1572	1339	701	81.35	84.12	82.22	1.07	5.978	9.73	473.84	148.3	120.3	28	63647	20553	84200	506625	3	0.4395	R 123
1588	1352	705.7	81.35	84.96	83.33	1.07	6.975	8.622	552.17	131.4	106.2	25.2	63647	20553	84200	506625	3.5	0.4395	R 123
1619	1375	714.6	81.35	86.48	85.34	1.07	9.964	7.241	876.56	110.41	88.84	21.57	63647	20553	84200	506625	5	0.4395	R 123
1207	827.9	117.6	80.99	88.34	87.68	0.05388	0.9964	0.0036	1.61	11.796	5.222	6.574	2994	1206	4200	810600	0.5	0.01975	R245fa
1395	950.9	119.5	80.99	89.17	88.84	0.05388	1.993	0.0032	4.74	10.418	4.284	6.134	2994	1206	4200	810600	1	0.01975	R245fa
1475	1002	120.2	80.99	89.45	89.23	0.05388	2.989	0.0031	9.26	9.982	3.987	5.995	2994	1206	4200	810600	1.5	0.01975	R245fa
1521	1031	120.6	80.99	89.59	89.42	0.05388	3.985	0.003	15.06	9.764	3.838	5.926	2994	1206	4200	810600	2	0.01975	R245fa
1551	1050	120.9	80.99	89.67	89.54	0.05388	4.982	0.0029	22.08	9.632	3.747	5.885	2994	1206	4200	810600	2.5	0.01975	R245fa
1207	824.2	292.4	80.99	83.36	80.68	0.2155	0.9964	0.1787	7.28	52.88	35.96	16.92	11977	4823	16800	810600	0.5	0.07898	R245fa
1395	959.7	305.3	80.99	86.68	85.35	0.2155	1.993	0.1081	14.64	32.02	20.59	11.43	11977	4823	16800	810600	1	0.07898	R245fa
1475	1017	310.2	80.99	87.79	86.9	0.2155	2.989	0.0948	26.15	28.1	17.74	10.36	11977	4823	16800	810600	1.5	0.07898	R245fa
1521	1050	312.9	80.99	88.34	87.68	0.2155	3.985	0.089	40.82	26.397	16.51	9.887	11977	4823	16800	810600	2	0.07898	R245fa
1551	1071	314.6	80.99	88.67	88.14	0.2155	4.982	0.0857	58.42	25.442	15.82	9.622	11977	4823	16800	810600	2.5	0.07898	R245fa
1521	1286	721.9	80.99	81.68	78.31	1.08	3.985	14.219	375.82	240.57	191.2	49.37	60030	24170	84200	810600	2	0.3958	R245fa
1551	1310	732.1	80.99	83.35	80.66	1.08	4.982	9.142	358.04	154.75	120.8	33.95	60030	24170	84200	810600	2.5	0.3958	R245fa
1572	1327	739.2	80.99	84.46	82.22	1.08	5.978	7.706	416.82	130.48	101.3	29.18	60030	24170	84200	810600	3	0.3958	R245fa
1588	1339	744.4	80.99	85.25	83.33	1.08	6.975	6.978	496.40	118.16	91.49	26.67	60030	24170	84200	810600	3.5	0.3958	R245fa
1619	1362	754.2	80.99	86.68	85.34	1.08	9.964	6.002	807.32	101.7	78.48	23.22	60030	24170	84200	810600	5	0.3958	R245fa